

6-1-2007

Understanding Coulomb effects in nanoscale Schottky-barrier-FETs

Klaus M. Indlekofer

Res Ctr Julich GmbH, Ctr Nanoelect Syst Informat Technol

Joachim Knoch

IBM Corp

Joerg Appenzeller

Birck Nanotechnology Center, Purdue University, appenzeller@purdue.edu

Follow this and additional works at: <http://docs.lib.purdue.edu/nanodocs>

 Part of the [Nanoscience and Nanotechnology Commons](#)

Indlekofer, Klaus M.; Knoch, Joachim; and Appenzeller, Joerg, "Understanding Coulomb effects in nanoscale Schottky-barrier-FETs" (2007). *Other Nanotechnology Publications*. Paper 169.
<http://docs.lib.purdue.edu/nanodocs/169>

This document has been made available through Purdue e-Pubs, a service of the Purdue University Libraries. Please contact epubs@purdue.edu for additional information.

Understanding Coulomb Effects in Nanoscale Schottky-Barrier-FETs

Klaus Michael Indlekofer, Joachim Knoch, and Joerg Appenzeller, *Senior Member, IEEE*

Abstract—We employ a novel multiconfigurational self-consistent Green's function approach (MCSCG) for the simulation of nanoscale Schottky-barrier-field-effect transistors (SB-FETs). This approach allows the calculation of electronic transport with a seamless transition from the single-electron regime to room-temperature FET operation. The particular improvement of the MCSCG stems from a self-consistent division of the channel system into a small subsystem of resonantly trapped states for which a many-body Fock space approach becomes numerically feasible and the rest of the system which can be treated adequately on a conventional mean-field level. The Fock space description allows for the calculation of few-electron Coulomb charging effects beyond the mean-field. We compare a conventional Hartree nonequilibrium Green's function calculation with the results of the MCSCG approach. Using the MCSCG method, Coulomb blockade effects are demonstrated at low temperatures while, under strong nonequilibrium and high-temperature conditions, the Hartree approximation is retained. Finally, the visibility of quantum and single-electron effects in scaled transistor structures is discussed.

Index Terms—Coulomb interaction, nanowire, Schottky-barrier-field-effect transistors (SB-FETs).

I. INTRODUCTION

ONE OF THE major challenges for the simulation of nanoscale field-effect transistors (FETs) consists of an adequate description of few-electron Coulomb blockade effects within the transistor channel: A proper simulation approach has to account for the Coulomb interaction of a few fluctuating electrons and, at the same time, has to be able to describe nonequilibrium quantum transport in an open nanosystem. Obviously, such effects are beyond the scope of a conventional mean-field simulation approach, which is based on a self-consistent Hartree potential for the description of the Coulomb interaction, albeit being able to account for quantum-confinement effects on the single-particle level. A many-body quantum approach becomes mandatory when it comes to the description of few-electron Coulomb blockade effects in ultimately scaled nanoFETs. While density-functional theory [1], in principle, is an exact *ab initio* many-body approach and can be used for the simulation of nanosystems [2], density-functional theory (DFT) normally aims at ground-state properties only. Furthermore,

realistic implementations of DFT typically employ the local-density approximation (LDA, and extensions thereof) and, thus, may exhibit mean-field artefacts. In general, an adequate description of few-electron Coulomb effects under application-relevant conditions thus requires the consideration of the Fock space as the general quantum-mechanical Hilbert space of a many-electron system [3], [4].

For the correct many-body description of the Coulomb interaction with the inclusion of contact coupling and nonequilibrium injection conditions, Fock space approaches such as real-time renormalization group (RTRG) [5], [6] or the Fock space Green's function [7] are available. This class of methods provides kinetic equations in Fock space, which include the Coulomb interaction and account for renormalization (i.e., energy shifts), level broadening (i.e., finite lifetimes of states), and dissipation (i.e., energy relaxation) due to the coupling to the contacts, at least to some extent. Since these approaches involve the 2^N -dimensional Fock space for the considered single-particle basis of N states, they typically are restricted to $N \lesssim 10$ for practical reasons. In the limit of small coupling, the Fock space description of the system can be approximated by a reduction to rate equations [8], [9], which deal with many-body eigenstates of the uncoupled Hamiltonian obtained via exact diagonalization [10]–[15] containing a full description of the Coulomb interaction.

Realistic modeling of a 1-D semiconductor nanotransistor typically involves a number N of single-particle states (orbitals or sites) of up to a few hundred, rendering a full numerical Fock space description impossible due to the exponential scaling of the resulting many-body space dimensions. Furthermore, most of the potentially current-carrying single-particle states are strongly coupled to the contacts, and thus, the picture of a weakly coupled system, in general, becomes inadequate. The nonequilibrium Green's function (NEGF) approach [16]–[20] in a mean-field approximation provides reasonable numerical scalability, however, in principle, lacks the description of few-electron Coulomb charging effects, which become apparent in the case of resonantly trapped states, in particular, at lower temperatures. A possible solution is the combination of the numerically well scaling mean-field NEGF with a Fock space description for those states where many-body Coulomb effects may become important for the device characteristics. In this context, we have recently proposed a multiconfigurational self-consistent Green's function approach (MCSCG) [15], [21] for the realistic simulation of nanodevice systems under application-relevant conditions with reasonable numerical efforts.

Manuscript received November 6, 2006; revised February 26, 2007. The review of this paper was arranged by Editor M. J. Deen.

K. M. Indlekofer and J. Knoch are with the Center of Nanoelectronic Systems for Information Technology, Research Centre Jülich GmbH, 52425 Jülich, Germany (e-mail: m.indlekofer@fz-juelich.de).

J. Appenzeller is with IBM T. J. Watson Research Center, Yorktown Heights, NY 10598 USA.

Digital Object Identifier 10.1109/TED.2007.895235

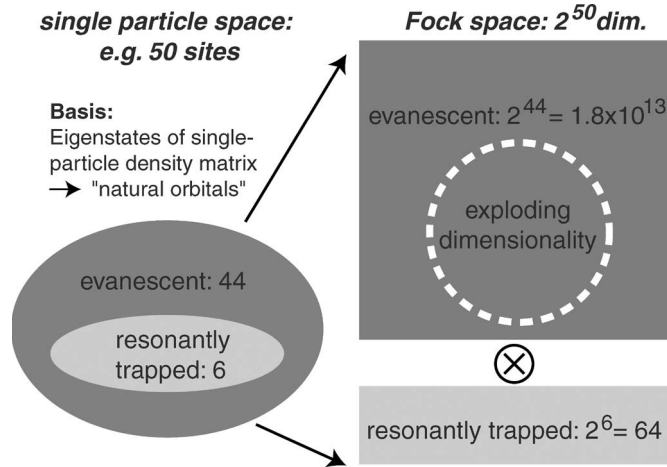


Fig. 1. Example for the division of the single-particle space (50 orbitals in the example) into two subspaces. For only resonantly trapped states (six in the example), a Fock space description is employed. The rest (evanescent) is treated by a mean-field description.

In the following sections, we will outline the main ideas and the algorithm behind the MCSCG and demonstrate its strengths by comparing a conventional Hartree NEGF calculation with the results of the MCSCG approach, providing significantly extended information to our recent conference contribution [22]. Using the MCSCG, Coulomb blockade effects are demonstrated at low temperatures while under strong nonequilibrium and high-temperature conditions the Hartree approximation is retained. Finally, the visibility of single-particle confinement and single-electron Coulomb effects in scaled nanowire-based transistor structures at room temperature will be discussed.

II. MULTICONFIGURATIONAL APPROACH

In order to handle systems with a large number N of single-particle states, the main idea of the MCSCG is to divide the system adaptively into two subsystems: resonantly trapped (i.e., weakly coupled) states and those states that couple strongly to the contacts, as depicted in Fig. 1. Within the subspace of $N' \lesssim 10$ resonantly trapped states, which require a many-body description of the Coulomb interaction, a Fock space method will be applied, whereas the rest ($N - N'$) is treated adequately on an approximated NEGF level. The eigenstates $\{|\kappa\rangle\}$ of the many-body statistical operator (or Hamiltonian, depending on the Fock space method) within the resonantly trapped subspace will be referred to as configurations with weights $\{w_\kappa\}$ corresponding to the respective eigenvalues. Thus, the configurations and their weights follow from a Fock space calculation, taking the detailed Coulomb interaction within this subspace into account. The many-body statistical operator ρ which describes the general thermodynamical state of the system [3] is assumed to be of the form

$$\rho = \sum_{\kappa} w_{\kappa} P_{\kappa} \otimes \rho_{\text{rest}}[\kappa] \quad (1)$$

where $P_{\kappa} \equiv |\kappa\rangle\langle\kappa|$ denotes the projection operator corresponding to the eigenstate $|\kappa\rangle$ and ρ_{rest} is the many-body statistical

operator of the rest, which may depend on the configuration κ . Motivated by this form, we define a configuration-averaged Green's function \bar{G} of the system as

$$\bar{G} = \sum_{\kappa} w_{\kappa} G[\kappa] \quad (2)$$

where $G[\kappa]$ corresponds to $P_{\kappa} \otimes \rho_{\text{rest}}[\kappa]$ and shall fulfill Dyson's equation [3], [4] with a suitable contact coupling plus Coulomb self-energy approximation $\Sigma[\kappa]$. In the simplest case, $\Sigma[\kappa]$ may be of a decoupled mean-field form [15], which is adequate for temperatures well above the corresponding Kondo temperature.

As for the Fock subspace of the resonantly trapped states, the projected many-body Hamiltonian contains the reduced single-particle and Coulomb terms. Furthermore, coupling to the contacts with nonequilibrium carrier injection and coupling (tunneling) to the rest of the system is described by means of self-energy kernels, depending on the chosen Fock space method. For the latter, various choices with different levels of sophistication are possible, for example: 1) Exact diagonalization with entropy maximization and Dyson's equation [3], [4] as subsidiary condition [15], [21]; 2) RTRG [5], [6]; or 3) Fock space Green's functions [7]. In the following, we will discuss the first option based on diagonalization. In this case, the many-body statistical operator is assumed to be diagonal in the eigenbasis of the resonant subspace Hamiltonian. Here, the eigenvalues w_{κ} are determined such that the resulting many-body Green's function G_{MB} in Lehmann representation fulfills Dyson's equation within the resonant subspace. In the simplest implementation, $\{w_{\kappa}\}$ is chosen such that the spectral peaks of $G_{\text{MB}}^<$ match those of $\bar{G}^<$ [15].

As an overall self-consistency condition, the resonantly trapped states experience a mean-field interaction of the rest, whereas the rest is subject to the set $\{\Sigma[\kappa]\}$ of self-energies originating from the resonant many-body configurations κ and its own mean-field interaction.

Finally, for the identification of resonantly trapped states, the single-particle eigenstates of the single-particle density-matrix are employed (so-called natural orbitals). The latter follows directly from the Green's function $\bar{G}^<$ as part of the multiconfigurational self-consistency procedure (note that each individual $G[\kappa]$ need not be self-consistent with its respective $\Sigma[\kappa]$). In turn, resonantly trapped states are defined as those single-particle eigenstates that exhibit a level broadening below a given threshold: Technically, if $-\Gamma(E)/2$ denotes the imaginary part of the coupling self-energy to the contacts [15], [18], an eigenstate $|n\rangle$ of the single-particle density-matrix with a mean energy E_n thus has to fulfill the criterion $\langle n|\Gamma(E_n)|n\rangle < \gamma_0$ in order to be identified as a "resonantly trapped" state, where γ_0 is the given threshold. As a further simplification, only those resonantly trapped states that exhibit occupation fluctuations require a full many-body treatment. Such fluctuations correspond to the eigenvalues of the single-particle density-matrix that deviate significantly from zero or one (i.e., a single-particle state that is fully occupied or always empty can be kept frozen in the electronic configuration). Hence, the

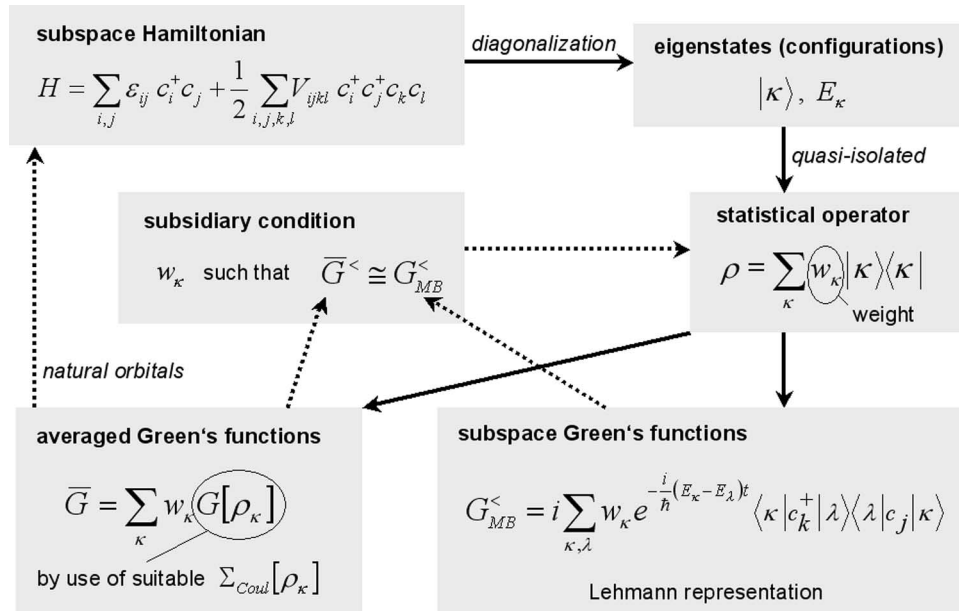


Fig. 2. Flowchart of the MCSCG algorithm. In the case shown, diagonalization is employed as the simplest Fock-subspace method. Arrows visualize the flow of the self-consistency loop.

single-particle basis, and its division into (relevant) resonantly trapped states and the rest is not predefined but follows adaptively from the MCSCG self-consistency loop as well. Fig. 2 illustrates the details of the algorithm as a flowchart.

For the calculation of expectation values of single-particle observables (e.g., electron density, current, spin density, etc.), the self-consistent Green's function $\bar{G}^<$ is employed as an approximation for the unknown exact $G^<$. Optionally, within the resonant subspace, one can use the many-body result (such as $G_{MB}^<$, the reduced statistical operator, dissipation kernel, etc.) for the evaluation of arbitrary expectation values, in particular, contour-ordered correlation functions of arbitrary order.

Analogous to other quantum-kinetic approaches, the detailed geometry of the simulated device structure and the underlying material parameters are expressed in terms of single- and two-particle matrix elements of the total many-body Hamiltonian. These matrix elements have to take the dielectric and electrode (image charge) screening into account. Depending on the desired accuracy, more or less sophisticated band structures (preferably formulated in a tight binding basis), such as the spin degree of freedom and spin-orbit coupling (Rashba and Dresselhaus terms), can be included. Even *ab initio* methods such as DFT [1] might be used to provide material-specific single-particle basis functions and associated matrix elements.

In summary, the MCSCG provides a systematic means to extend the well-established mean-field NEGF simulation technique, incorporating many-body interaction terms in order to describe few-electron charging effects. On the other hand, in contrast to a numerically unfeasible full many-body description of the realistic device structure, the MCSCG provides a significant reduction of degrees of freedom, focusing adaptively on the relevant many-body states. In comparison to the commonly employed idealized many-body models which require user-supplied constants (such as capacitances or gate-efficiency factors), the MCSCG implicitly provides effective parameters for

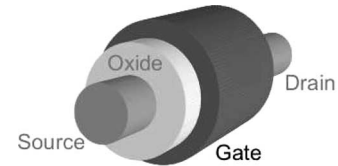


Fig. 3. Schematic sketch of a nanowire MOSFET with coaxial gate.

relevant states, which follow adaptively from the given realistic device structure, and, in general, are nonlinear functions of the external electrode voltages.

III. SIMULATION OF NANOWIRE SB-FETs

In order to demonstrate the strengths of the MCSCG approach, we consider a 1-D coaxially gated nanowire transistor with Schottky-barrier source and drain contacts [26]–[28], since deviations from a mean-field approximation become most apparent in a system with quasi-bound states. Fig. 3 shows a schematic of such a nanowire transistor, where we assume a channel length of $L = 20$ nm, a diameter of $d_{ch} = 4$ nm, and a gate oxide thickness of $d_{ox} = 10$ nm. We employ a one-band tight-binding description with one lateral channel mode only (a tight-binding basis provides a flexible and accurate way to describe nanoscale device structures in real space [16], [18]). Since the spin degree of freedom is included and a site spacing of $a = 1$ nm is employed, we thus consider $N = 40$ single-particle states. Such a nanowire transistor can, in principle, be realized with a semiconducting InGaAs nanowire with SiO_2 as gate dielectric.

It has been shown that the electrostatics of coaxially gated nanowire transistors can be well described by a modified 1-D Poisson equation [29], accounting for the screening effects due to the gate electrode. This Poisson equation allows to easily

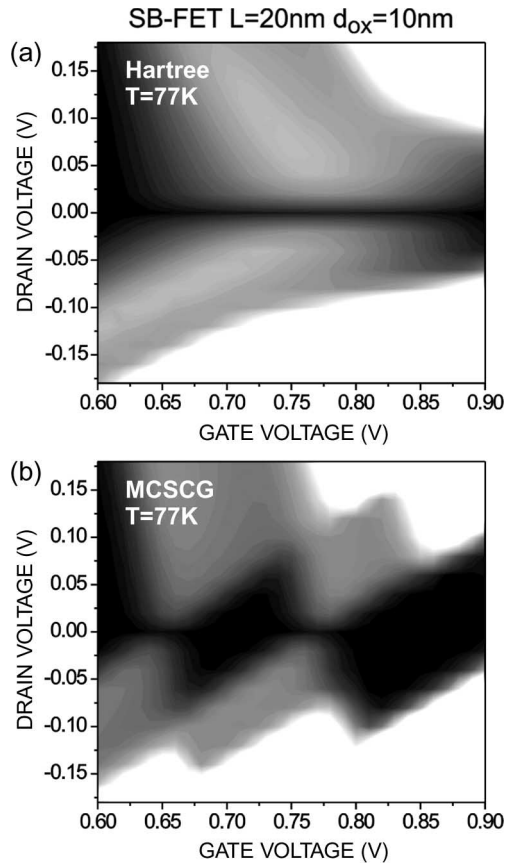


Fig. 4. Nonlinear grayscale plot of the total drain-current for the SB-FET at $T = 77$ K (black = 0 nA, white = 5 nA). (a) Hartree-only case. (b) MCSCG case: Coulomb diamonds arise.

calculate the Coulomb Green's function, which in turn enables the description of the classical electrostatics and the screened interaction between electrons on equal footing [15]. Within the scope of the MCSCG approach, the realistic influence of the external electrodes (gate, source, and drain) is inherently contained within the single-particle potential of the channel. In contrast to highly idealized impurity-like models of Coulomb blockade, a change in the electrode voltages does not only provide a shifted or tilted potential profile but may also result in a spatially modified shape of the potential and, in turn, altered wavefunctions. Therefore, the few-electron energy spectrum and, thus, the transport properties, in general, become a nonlinear function of all applied voltages.

For the following simulation results, the simplest MCSCG variant has been employed, based on diagonalization (with $N' = 6$ resonantly trapped states yielding 64 Fock space dimensions) with a decoupled static self-energy form.

Fig. 4 visualizes the simulated drain-current I_D for the single-electron transport regime ($T = 77$ K) as a grayscale plot. In contrast to the Hartree-only calculation [Fig. 4(a)], the MCSCG approach [Fig. 4(b)] correctly reveals diamondlike-shaped patterns due to the quantized Coulomb interaction (as predicted by the orthodox theory and observed in experiments [24], [25]). While the MCSCG treatment is able to cope with the mixture of many-body configurations, the Hartree theory

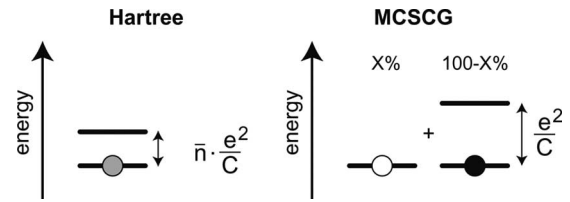


Fig. 5. Visualization of the difference between the mean-field (Hartree) and the many-body (MCSCG) description of Coulomb interaction of resonantly trapped states. \bar{n} denotes the average electron number.

only provides a mean interaction potential for the description of the Coulomb interaction.

The origin of the difference between the many-body description of the Coulomb interaction and its mean-field-approximated version can be understood as follows. Assuming an average electron number \bar{n} inside the resonantly trapped states, the mean-field picture provides an overall shift of single-particle energies by $\propto \bar{n}e^2/C$, where \bar{n} need not be an integer. This situation is schematically shown in Fig. 5 (left). In contrast, the many-body state (roughly spoken) consists of a quantum ensemble of many-body configurations with integer electron numbers each, hence, providing only weighted realizations of full-interaction energies, as depicted in the right part of Fig. 5. As a result, Coulomb oscillations arise. Apparently, this difference between the many-body picture and the mean-field approximation becomes significant at low temperatures for resonantly trapped single-particle states that exhibit a small level broadening (as compared to the spacing e^2/C). On the other hand, in the high-temperature limit and for states with strong coupling to the environment (i.e., strong broadening), the many-body and the mean-field description converge: Here, a weighted average of peaks with spacing e^2/C becomes equivalent to a shift of the mean energy. Indeed, the MCSCG approach consistently employs the many-body description for resonantly trapped states only.

Fig. 6 shows $I_D(V_{GS})$ curves for different drain voltages V_{DS} . In the MCSCG case [Fig. 6(b)], single-electron transport can be identified in terms of Coulomb oscillations for the two lowest V_{DS} , whereas the Hartree-only simulation [Fig. 6(a)] lacks these features; the Hartree-only case exhibits broader peaks solely due to the single-particle levels of the system. However, with increasing V_{DS} , both approaches become equivalent (note that the subthreshold regime shows the regular behavior and has been omitted here).

Finally, Fig. 7 shows the room-temperature ($T = 300$ K) characteristics. Apart from the slight modulation in the MCSCG calculation [Fig. 7(b)], which is a remnant of the Coulomb oscillation, the Hartree [Fig. 7(a)] and MCSCG [Fig. 6(b)] results are in good agreement.

IV. COULOMB EFFECTS AND SCALING OF NANOWIRE FETs

In this section, we discuss the relevance of few-electron Coulomb charging effects for room-temperature nanowire-FET devices. Two effects become important with the downscaling

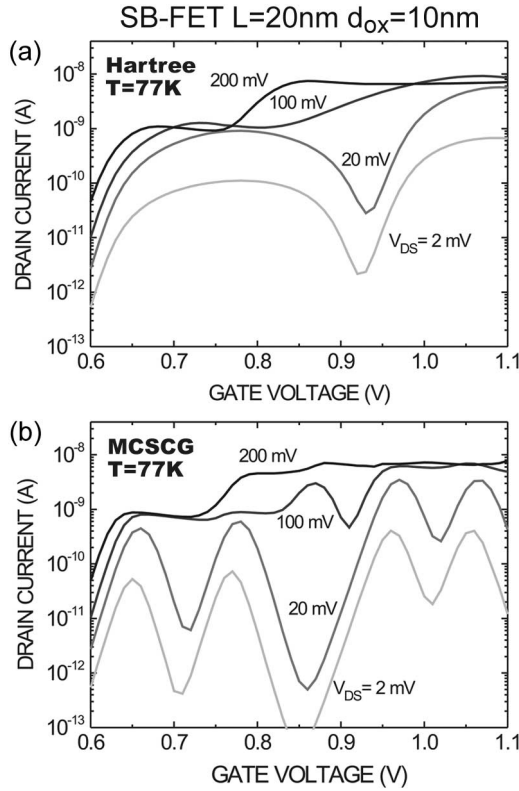


Fig. 6. SB-FET transfer characteristics at $T = 77$ K. (a) Hartree-only. (b) MCSCG approach: Coulomb oscillations are clearly visible.

of the channel length L : 1) The longitudinal single-particle quantization splitting

$$\Delta E \propto \frac{\hbar^2}{m^* L^2} \quad (3)$$

of states inside the channel. The lateral quantization energy $\propto d_{\text{ch}}^{-2}$ is not considered here, leading only to an overall shift of energy bands for a constant channel diameter d_{ch} . 2) The single-electron Coulomb charging energy

$$E_C = \frac{e^2}{C^*}. \quad (4)$$

The effective total capacitance C^* is proportional to the classical total capacitance of the channel [21], however, with a proportionality factor which, in general, also depends on L , d_{ox} , the electron number, and other parameters due to quantum effects. In principle, this factor has to be determined from the many-body quantum calculations, as was discussed in the study in [21].

If we define measures $\Delta E/k_B T$ for the visibility of single-particle quantization and $E_C/k_B T$ for the visibility of few-electron charging effects (i.e., Coulomb oscillations), it is apparent that $\Delta E/k_B T \propto m^{*-1} L^{-2}$ becomes larger with smaller channel length L and smaller m^* due to an increased quantization energy. In contrast, $E_C/k_B T$ depends, in particu-

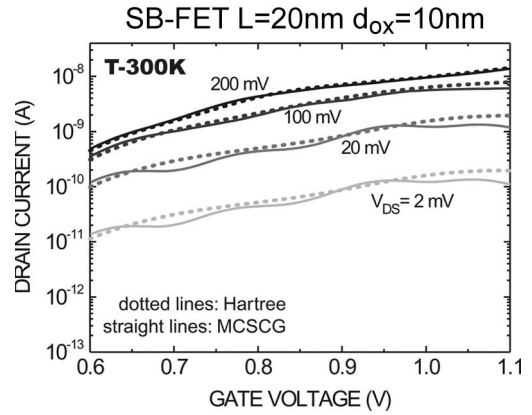


Fig. 7. SB-FET transfer characteristics at $T = 300$ K. Solid lines: MCSCG approach: Only weak remnants of the Coulomb oscillations can be seen. Dotted lines: Hartree-only.

lar, on the scaling of C_{ox} , where in a cylindrical surrounding-gate transistor, we have

$$C_{\text{ox}} = \frac{\pi \epsilon_0 \epsilon_{\text{ch}} d_{\text{ch}}^2 L}{4 \lambda^2}. \quad (5)$$

Here, λ is the screening length of the device. Electrostatic integrity in a transistor is preserved as long as the screening by the gate is sufficiently strong, or in other words, if $\lambda \ll L$ (as a side-effect, the limit $\lambda/L \rightarrow 0$ implies a strong screening of the Schottky barriers by the gate, leading to a more transparent source and drain contacts [23]). To be specific, λ is given by [29]

$$\lambda^2 = \frac{\epsilon_{\text{ch}}}{\epsilon_{\text{ox}}} \frac{d_{\text{ch}}^2}{8} \ln \left(1 + 2 \frac{d_{\text{ox}}}{d_{\text{ch}}} \right) \quad (6)$$

which means that C_{ox} and, hence, the visibility of Coulomb effects $E_C/k_B T$ depends on all three geometrical lengths: L , d_{ox} , and d_{ch} . As a result, there is no universal scaling of Coulomb effects in L . In order to determine the scaling law for $E_C/k_B T$, one, therefore, has to specify the experimentally chosen scaling of d_{ox} and d_{ch} with varying L .

Three application-relevant scaling cases for a nanowire-based FET can be distinguished [note that, in the following estimations, we assume $C^*/C_{\text{ox}} = \text{const}$ for simplicity, thus neglecting the variation of the quantum confinement factor in C^* (cf. [21]) and the source and drain capacitances].

- 1) Proportional scaling of all geometrical lengths: As was aforementioned, preserving electrostatic integrity when scaling down L requires also a scaling of λ by decreasing d_{ch} and d_{ox} (and/or increasing ϵ_{ox}). If we scale all geometrical lengths by the same factor as the channel length L , we obtain an approximated scaling law $E_C/k_B T \propto L^{-1}$ for the visibility of Coulomb charging effects. Comparing the approximate scaling laws $E_C/k_B T \propto L^{-1}$ and $\Delta E/k_B T \propto L^{-2}$ for the Coulomb and single-particle quantization energies, respectively, one can see that below a critical channel length, the single-particle quantization becomes the dominating energy scale (as long as m^* and other parameters are kept

constant). Nevertheless, within this simple approximation, the temperature below which Coulomb effects become visible increases with decreasing channel lengths, and thus, such effects may eventually become relevant at room temperature.

- 2) Scaling of L alone: The same scaling law $E_C/k_B T \propto L^{-1}$, as for case 1), can also be derived for an FET where d_{ox} and d_{ch} are kept constant (hence, $\lambda = \text{const}$ as well) with varying L . Note, however, that once the short-channel regime is reached (that is $\lambda \ll L$ is no longer fulfilled), the source and drain capacitance will gain influence, thus terminating the L^{-1} scaling of $E_C/k_B T$ in this case.
- 3) Scaling of L and $\lambda(d_{ox})$: An interesting scaling law for the Coulomb energy, and hence, its visibility arises for the case that the channel diameter d_{ch} is kept constant. Such a situation can occur for nanowire FETs based on carbon nanotubes or semiconductor whiskers. Assuming electrostatic integrity (that is $\lambda \ll L$) with a scaling of d_{ox} (and/or ϵ_{ox}) such that $\lambda(d_{ox}) \propto L$, we obtain a reciprocal scaling law $E_C/k_B T \propto L$ as compared to the cases discussed above. Here, the capacitance increases with decreasing L . Consequently, the Coulomb charging energy and, hence, the temperature below which Coulomb effects become visible decreases with downscaling of the channel length. In such a peculiar situation, single-electron charging effects become irrelevant at room temperature for downscaled devices. Note, however, that single-particle quantization effects would still scale as L^{-2} .

An important point has not yet been addressed, namely, the relation between the onset of short-channel effects (i.e., $\lambda \ll L$ is no longer fulfilled) and the visibility of Coulomb effects. Indeed, the above discussion does not imply a general correlation between these two. Of course, short-channel effects imply a reduced gate efficiency, however, they do not necessarily yield small capacitances (and, hence, large Coulomb energies). This can easily be understood by the following argument. Equivalent to specifying L , d_{ox} , and d_{ch} , one can also choose L , λ/L , and C^* as the three independent parameters (as long as C^* is not limited by the source and drain capacitances). Consider, for instance, an artificial set of FETs with a fixed C^* and L but varying λ/L . It is obvious that all these devices have the same visibility measure $E_C/k_B T$ but cover the whole range from electrostatically well behaved (i.e., $\lambda \ll L$) to the opposite extreme of short-channel FETs.

The MCSCG approach can handle all situations mentioned above, accounting for single-particle quantization and few-electron Coulomb effects. In order to visualize our statements, we will now discuss two opposite scaling examples, both starting from the previously discussed SB-FET of Section III with $L = 20$ nm and an oxide thickness of $d_{ox} = 10$ nm. The transfer characteristics of this device were shown in Fig. 7. The two scaled SB-FETs (a) and (b) that we want to discuss now exhibit both a downscaled channel length of $L = 15$ nm with an unchanged fixed diameter. The first device (a) is scaled according to case 2) (with an unchanged rather large gate oxide

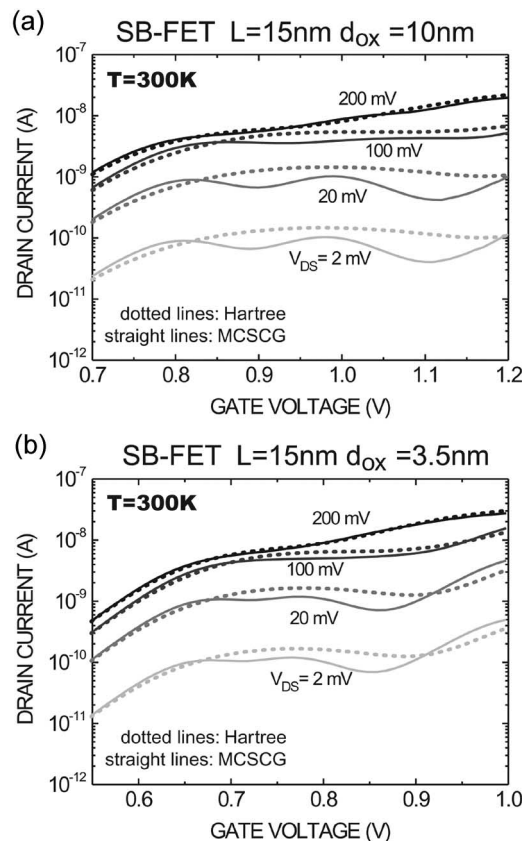


Fig. 8. SB-FET transfer characteristics at $T = 300$ K with different d_{ox} in (a) and (b). Solid lines: MCSCG approach. Dotted lines: Hartree-only. For the short-channel device (a) with the smaller capacitance, Coulomb oscillations are important even at room temperature.

thickness of $d_{ox} = 10$ nm), whereas the second device (b) is scaled according to case 3) with a reduced $d_{ox} = 3.5$ nm, such that $\lambda \propto L$, leading to screening lengths of $\lambda_a = 3.71$ nm and $\lambda_b = 2.79$ nm, respectively. This implies that device (a) exhibits short-channel effects, whereas the second transistor (b) is an electrostatically well-tempered device. Fig. 8(a) shows room-temperature transfer characteristics of the device (a) for different V_{DS} , and Fig. 8(b) shows the same for the device (b) with the thinner gate oxide.

As shown in Fig. 8(a) for device (a), significant differences between the Hartree and the MCSCG calculation can be observed with a well-pronounced additional modulation of the drain-current, in particular, at low V_{DS} . This modulation stems from single-electron Coulomb charging effects with $E_C \approx 96$ meV for the first two electrons. The latter value has to be compared to $E_C \approx 93$ meV of the unscaled FET. At a first look, this almost negligible change in E_C appears surprising since device (a) corresponds to the scaling case 2), where $C_{ox} \propto L$. The reason for this saturation in E_C for the short-channel FET (a), however, can be found in the increased influence of the drain and source capacitance on C^* , as discussed in case 2). Nevertheless, comparing Figs. 7 and 8(a), the gate voltage interval for one Coulomb oscillation is increased with the reduction of L . In our case, this has to be attributed to a reduced gate efficiency due to short-channel effects.

In contrast, for the electrostatically well-tempered device (b) with a significantly smaller $E_C \approx 66$ meV [with $E_C \propto L$

approximately, see case 3)], the Hartree and the MCSCG approach yield similar results. A Coulomb oscillation at $V_G \approx 0.72$ V is still visible in Fig. 8(b), however, exhibiting a reduced amplitude as compared to Figs. 7 and 8(a). The modulations in the Hartree and MCSCG results are dominated by the single-particle quantization; the differences between the Hartree-only case and the MCSCG (in particular, a slight shift in gate voltage) result mainly from Coulomb exchange terms, which are neglected in the Hartree approximation. Finally, the increase in drain-current of FET (b) stems from the thinner effective Schottky barriers due to a reduced λ (see [23]).

In conclusion, single-particle quantization effects have an increasing influence on the room-temperature characteristics with decreasing channel lengths, scaling as L^{-2} . In contrast, the scaling of the visibility of few-electron charging effects at room temperature strongly depends on the chosen system-parameter scaling. For the commonly employed proportional scaling of all geometrical lengths, Coulomb energies increase as L^{-1} , thus becoming more important for smaller devices. Nevertheless, the single-particle quantization will dominate below a characteristic channel length. Even for the case that few-electron charging effects are not visible at room temperature, low-temperature measurements are often used to extract the effective capacitances from Coulomb diamonds. Also, in this case, a Fock space simulation approach becomes mandatory, seamlessly covering the room-temperature operation and the Coulomb blockade regime to obtain consistent (i.e., comparable) results. Here, the MCSCG provides a numerically efficient many-body simulation technique.

V. CONCLUSION

In summary, we have compared the conventional Hartree NEGF with the MCSCG and have shown that the multiconfigurational approach is able to describe single-electron charging effects in the low-temperature limit for a realistic FET structure. In case of strong nonequilibrium (with an almost depleted channel) and high-temperature conditions, the MCSCG and the well-established Hartree approximation lead to equivalent results for the discussed example of a nanowire MOSFET. As such, the MCSCG yields a seamless transition from the single-electron transport regime to transistor operation at room temperature. For realistic FETs with a large number of sites where a full Fock space formulation becomes impossible, the MCSCG permits a self-consistent Fock space treatment of states which are responsible for few-electron charging effects. Finally, we have shown that the scaling law for the visibility of Coulomb effects at room temperature strongly depends on the chosen relative scaling of geometrical lengths.

REFERENCES

- [1] R. Dreizler and E. Gross, *Density Functional Theory*, For a review see (and references therein). New York: Plenum, 1995.
- [2] A. Wensauer, O. Steffens, M. Suhrke, and U. Rössler, "Laterally coupled few-electron quantum dots," *Phys. Rev. B, Condens. Matter*, vol. 62, no. 4, pp. 2605–2613, Jul. 2000.
- [3] A. L. Fetter and J. D. Walecka, *Quantum Theory of Many-Particle Systems*. New York: McGraw-Hill, 1971.
- [4] G. D. Mahan, *Many-Particle Physics*. New York: Plenum, 1990.
- [5] H. Schoeller and J. König, "Real-time renormalization group and charge fluctuations in quantum dots," *Phys. Rev. Lett.*, vol. 84, no. 16, pp. 3686–3689, Apr. 2000.
- [6] H. Schoeller, "An introduction to real-time renormalization group," *Lect. Notes Phys.*, vol. 544, pp. 137–166, 2000. cond-mat/9909400.
- [7] S. Datta, *Fock Space Formulation for Nanoscale Transport*. cond-mat/0603034.
- [8] C. W. Beenakker, "Theory of Coulomb-blockade oscillations in the conductance of a quantum dot," *Phys. Rev. B, Condens. Matter*, vol. 44, no. 4, pp. 1646–1656, Jul. 1991.
- [9] S. A. Gurvitz, "Rate equations for quantum transport in multi-dot systems," *Phys. Rev. B, Condens. Matter*, vol. 57, no. 11, p. 6602, 1997.
- [10] S. M. Reimann and M. Manninen, "Electronic structure of quantum dots," *Rev. Mod. Phys.*, vol. 74, no. 4, pp. 1283–1342, Nov. 2002.
- [11] D. Pfannkuche and S. E. Ulloa, "Selection rules for transport excitation spectroscopy of few-electron quantum dots," *Phys. Rev. Lett.*, vol. 74, no. 7, pp. 1194–1197, Feb. 1995.
- [12] R. Rinaldi, S. Antonaci, M. DeVittorio, R. Cingolani, U. Hohenester, E. Molinari, H. Lipsanen, and J. Tulkki, "Effects of few-particle interaction on the atomiclike levels of a single strain-induced quantum dot," *Phys. Rev. B, Condens. Matter*, vol. 62, no. 3, pp. 1592–1595, Jul. 2000.
- [13] E. Biolatti, I. D'Amico, P. Zanardi, and F. Rossi, "Electro-optical properties of semiconductor quantum dots: Application to quantum information processing," *Phys. Rev. B, Condens. Matter*, vol. 65, no. 7, pp. 075 306–075 328, Jan. 2002.
- [14] K. M. Indlekofer and H. Lüth, "Many-particle density-matrix approach to a quantum dot system for the strong electron accumulation case," *Phys. Rev. B, Condens. Matter*, vol. 62, no. 19, pp. 13 016–13 021, Nov. 2000.
- [15] K. M. Indlekofer, J. Knoch, and J. Appenzeller, "Quantum kinetic description of Coulomb effects in one-dimensional nanoscale transistors," *Phys. Rev. B, Condens. Matter*, vol. 72, no. 12, pp. 125 308-1–125 308-7, Sep. 2005.
- [16] S. Datta, *Electronic Transport in Mesoscopic Systems*. Cambridge, U.K.: Cambridge Univ. Press, 1998.
- [17] D. K. Ferry and S. M. Goodnick, *Transport in Nanostructures*. Cambridge, U.K.: Cambridge Univ. Press, 1997.
- [18] R. Lake, G. Klimeck, R. C. Bowen, and D. Jovanovic, "Single and multi-band modeling of quantum electron transport through layered semiconductor devices," *J. Appl. Phys.*, vol. 81, no. 12, pp. 7845–7869, 1997.
- [19] J. Guo, S. Datta, and M. Lundstrom, "A numerical study of scaling issues for Schottky barrier carbon nanotube transistors," *IEEE Trans. Electron Devices*, vol. 51, no. 2, pp. 172–177, Feb. 2004.
- [20] D. L. John and D. L. Pulfrey, "Green's function calculations for semi-infinite carbon nanotubes," *Phys. Stat. Sol. B*, vol. 243, no. 2, pp. 442–448, 2006.
- [21] K. M. Indlekofer, J. Knoch, and J. Appenzeller, "Quantum confinement corrections to the capacitance of gated one-dimensional nanostructures," *Phys. Rev. B, Condens. Matter*, vol. 74, no. 11, pp. 113 310–113 313, Sep. 2006.
- [22] K. M. Indlekofer, J. Knoch, and J. Appenzeller, "Seamless transition from the single-electron regime to field-effect transistor operation of nanoscale Schottky-barrier FETs," in *Proc. 64th Device Res. Conf.*, 2006, pp. 253–254. IEEE 06TH8896.
- [23] J. Knoch and J. Appenzeller, "Impact of the channel thickness on the performance of Schottky barrier metal-oxide-semiconductor field-effect transistors," *Appl. Phys. Lett.*, vol. 81, no. 16, pp. 3082–3084, Oct. 2002.
- [24] M. Suzuki, K. Ishibashi, K. Toratani, D. Tsuya, and Y. Aoyagi, "Tunnel barrier formation using argon-ion irradiation and single quantum dots in multiwall carbon nanotubes," *Appl. Phys. Lett.*, vol. 81, no. 12, pp. 2273–2275, Sep. 2003.
- [25] C. Thelander, T. Martensson, M. T. Björk, B. J. Ohlsson, M. W. Larsson, L. R. Wallenberg, and L. Samuelson, "Single-electron transistors in heterostructure nanowires," *Appl. Phys. Lett.*, vol. 83, no. 10, pp. 2052–2054, Sep. 2003.
- [26] J. R. Barker and D. K. Ferry, "On the physics and modeling of small semiconductor devices—II: The very small device," *Solid State Electron.*, vol. 23, no. 6, pp. 531–544, Jun. 1980.
- [27] J. R. Tucker, C. Wang, and P. S. Carney, "Silicon field-effect transistor based on quantum tunneling," *Appl. Phys. Lett.*, vol. 65, no. 5, pp. 618–620, Aug. 1994.
- [28] Q. T. Zhao, F. Klinkhammer, M. Dolle, L. Kappius, and S. Mantl, "Nanometer patterning of epitaxial CoSi₂/Si(100) for ultrashort channel Schottky barrier metal-oxide-semiconductor field effect transistors," *Appl. Phys. Lett.*, vol. 74, no. 3, p. 454, 1998.
- [29] C. P. Auth and J. D. Plummer, "Scaling theory for cylindrical, fully-depleted, surrounding-gate MOSFET's," *IEEE Electron Device Lett.*, vol. 18, no. 2, pp. 74–76, Feb. 1997.



Klaus Michael Indlekofer received the Dipl.-Phys. (*summa cum laude*) and Dr.rer.nat. degrees (*summa cum laude*) in physics from the Rheinisch-Westfälischen Technischen Hochschule (RWTH) Aachen University, Aachen, Germany, in 1996 and 1999, respectively.

These works were carried out in the Research Centre Juelich, Juelich, Germany, and focused on experimental as well as theoretical aspects of single-electron effects in vertical III/V resonant tunneling transistors. From 2000 to 2001, he was involved in the development of the “WinGreen” transport simulation tool. From 2001–2002, he worked on transport models for open quantum-dot systems in the Department of Electrical Engineering, Arizona State University, as a Feodor-Lynen Fellow (A. v. Humboldt Foundation). In 2002, he returned to the Research Centre Juelich and is currently the Leader of a research group developing many-body real-time models for Coulomb effects in nanodevices.



Joerg Appenzeller (M'02–SM'04) received the M.S. and Ph.D. degrees in physics from the Technical University of Aachen, Aachen, Germany, in 1991 and 1995, respectively.

His Ph.D. dissertation investigated quantum-transport phenomena in low dimensional systems based on III/V heterostructures. He worked for one year as a Research Scientist in the Research Center in Juelich, Germany, before he became an Assistant Professor with the Technical University of Aachen in 1996. During his professorship, he explored mesoscopic electron transport in different materials including carbon nanotubes and superconductor/semiconductor-hybrid devices. From 1998 to 1999, he was with the Massachusetts Institute of Technology, Cambridge, as a Visiting Scientist, exploring the ultimate scaling limits of silicon MOSFET devices. Since 2001, he has been with the IBM T. J. Watson Research Center, Yorktown Heights, NY, as a Research Staff Member mainly involved in the investigation of the potential of carbon nanotubes for a future nanoelectronics.



Joachim Knoch received the M.S. and Ph.D. degrees in physics from the Technical University of Aachen, Aachen, Germany, in 1998 and 2001, respectively.

At the University of Aachen, he investigated quantum transport in superconductor/semiconductor hybrids based on III–V heterostructures, as well as worked on the modeling and realization of ultrashort-channel silicon MOSFETs. From September 2001 to December 2002, he was with the Microsystems Technology Laboratory, Massachusetts Institute of Technology, Cambridge, where he worked on InP-HEMT devices. In 2003, he was with the Institute of Thin Films and Interfaces, Research Center Juelich, Germany, as a Research Scientist and was involved in the exploration of electronic transport in alternative field-effect transistor devices, such as carbon nanotube field-effect transistors and ultrathin-body Schottky-barrier devices. Since December 2006, he has been with the IBM Research GmbH, Zurich Research Laboratory, Rueschlikon, Switzerland, as a Research Staff Member working on nanowire field-effect transistors.